Reactive sputtered ZnO thin films: Influence of the O_2/Ar flow ratio on the oxygen vacancies and paramagnetic active sites

Adrián A. Camacho-Berríos[a, *], Víctor M. Pantojas[b], Wilfredo Otaño[b]

[a]*Physics, University of Puerto Rico, San Juan, Puerto Rico, 00925, USA*

[b]*Mathematics-Physics, University of Puerto Rico, Cayey, Puerto Rico, 00736, USA*

Abstract

Zinc oxide thin films were prepared under oxygen-deficient and oxygen-rich conditions by changing the oxygen to argon ratio (O_2/Ar) during the reactive sputtering deposition at room temperature. The effects of increasing the partial pressure of oxygen in the sputtering gas from 20 to 70 % O_2/Ar on the thin film composition, crystallinity and defects that can act as active sites for gas reactions were studied using X-rays diffraction, X-rays photoelectron spectroscopy (XPS), Raman scattering and electron paramagnetic resonance (EPR). All the films exhibited a textured (0002) wurtzite phase and a crystallite size that increases as the partial pressure of oxygen in the sputtering gas increases. The XPS analysis showed that the number of oxygen vacancies decreases as the oxygen percent in the sputtering gas increases. The Raman spectra of the samples contained a band related to a hydroxide, OH, bond in addition to the vibrational modes associated with the wurtzite structure. A strong EPR signal, consistent with the OH acting as a paramagnetic center, was detected in all the films. An additional, but very weak EPR peak, was observed in the film grown at 20 % O_2/Ar, which was assigned to singly ionized oxygen vacancies located in the crystallite lattice. These paramagnetic centers are highly reactive because of their unpaired electrons and their formation will have important effects on the physical and chemical properties of the thin films.

Keywords: Active site**,** Paramagnetic defect**,** Zinc oxide, thin film**,** Reactive sputtering**,** Oxygen vacancy

---

[*] Corresponding author.
E-mail address: adrian.camacho@upr.edu
Present address: Department of Mathematics-Physics, 205 Antonio R. Barceló, Room 124 New Building of Science, Cayey, Puerto Rico 00736

1. Introduction

Zinc oxide (ZnO) nanomaterials are of great interest in the fields of photocatalysis and gas sensors due to its physical and chemical properties [1–3]. For example, the surface has good adsorption properties and is highly reactive due to presence oxygen vacancies (V_O) [4]. However, it has been pointed out that even though ZnO is sensitive to the presence of impurity gases in air, its performance is limited due to its low selectivity [5].

The nature and concentration of active sites can determine the type of interaction between the material and the gas molecules, thus modifying the selectivity of the sensor. Active sites can be a single atom, groups of atoms, molecules, or structural defects such as interstitials and vacancies. Depending on their chemical nature, active sites can be classified as acid-base, oxidation-reduction or paramagnetic centers. For example, chemisorbed oxygen such as O^- act as an oxidative site [6]. Paramagnetic centers are of special interest because they are highly reactive due to their unpaired electrons [5,7]. Examples of paramagnetic centers that fall into the active site category are some OH groups and paramagnetic defects, such as singly ionized oxygen vacancies (V_O^+) [8].

Electron paramagnetic resonance (EPR) is an excellent technique to investigate defects with unpaired electrons in semiconductors. It has been used to identify defects centers such as V_O^+ in ZnO nanostructures: nanowires [9], nanoparticles [10–12] nanoflowers [13], quantum dots [14], tetrapod [15], and single crystal [16]. However, EPR have not been used in any study to characterize paramagnetic defects in ZnO thin films prepared by magnetron sputtering [17], where the presence and relative abundance of V_O^+ will be of great interest.

In this work, ZnO thin films were deposited by the DC pulsed magnetron sputtering technique. Several advantages of this technique include working with high-purity metal targets to reduce the amount of impurities in the films and the growth of homogenous films over large areas. Also, sputtered films can be prepared in a variety of substrates such as sapphire, glass and silicon or be deposited on top of interdigital transducers to make sensor devices.

For sputtering deposition, several plasma-process parameters are controlled including sputtering power, substrate temperature, deposition pressure, target-to-substrate distance, and sputtering gas composition. The sputtering gas composition, in particular, can be used to change the stoichiometry of the films and their structural, optical, and electrical properties [18–22]. Therefore, the influence of different O_2/Ar ratios on the V_O formation, and consequent characteristics of the films such as crystal structure, morphology and composition, is studied. By using a combination of XPS and EPR, changes in the number of V_O and the possible formation of V_O^+ species are observed. Additionally, the presence of OH groups is confirmed by Raman spectroscopy and EPR.

2. Experimental details

ZnO thin films were grown by reactive magnetron sputtering. One advantage of reactive sputtering is the use of high-purity zinc metal as a target (99.999 %) to grow a compound material such as ZnO. Undoped silicon (100) substrates were heated at T = 1000 ºC for 24 hours in air to grow an oxide layer. The substrates were ultrasonically cleaned in deionized water followed by ethanol and acetone for five minutes each and dried using nitrogen gas. The sputtering chamber was evacuated to a base pressure on the order of 10^{-5} Pa prior to deposition. The target-to-substrate distance was kept at 4 cm. The deposition pressure was set to 1.33 Pa, and the sputtering power was set to 40 W using a pulsed DC power supply. The one-inch zinc target was cleaned by pre-sputtering the chamber with argon gas for 5 minutes. The initial substrate temperature was T_{sub} = 25 °C, which was monitored using a thermocouple placed near the substrate. The thickness of the film was measured with an Alpha Step IQ surface profiler (KLA Tencor) at several places and then averaged. The deposition rate was calculated by dividing the film thickness by the sputtering time. The deposition time was adjusted to obtain a film thickness of 502±26 nm. The oxygen and argon flows were controlled using two mass flow controllers. Table I summarizes the growth conditions of the films.

The structural properties of the thin films were examined by X-ray diffraction (XRD) using a Rigaku SmartLab X-ray diffractometer (Rigaku, USA) with Cu K_{α} radiation in parallel beam configuration. Room-temperature Raman measurements were performed using a DXR Raman microscope (ThermoFisher Scientific, USA) at an excitation wavelength of 532 nm. The surface morphology and grain size were studied by scanning electron microscopy (SEM) with a JEOL JSM-6360 (JEOL, Japan). The SEM acceleration voltage and working distance were set to 20kV, and 9 mm respectively. Surface composition and chemical information was obtained by X-ray photoelectron spectroscopy (XPS) using a PHI 5600 (Physical Electronics Inc., USA) with an Al Kα (hν = 1486.6 eV) monochromatic X-ray source with a power of 350 W and pass energy of 58.70 eV. The XPS measurements were recorded at room temperature and a base pressure of around 6.6 x10-7 Pa. No ion sputtering was performed prior the XPS measurements. The binding energies were calibrated using the carbon C1s peak (284.e eV) as reference. The EPR absorption spectra were measured at room temperature using a Bruker EMX (Bruker, USA) spectrometer at a frequency of 9.45 GHz, a magnetic field modulation of 100 kHz and a modulation amplitude of $1x10^{-4}$ T.

3. Results and discussion

Figure 1 shows the deposition rate of the ZnO thin films as a function of the O_2/Ar ratio. The deposition rates ranged between 4 ± 0.17 and 5.56 ± 0.12 nm/min depending on the deposition conditions. Literature reports of deposition rates under similar conditions of reactive sputtering are between 2.5 nm/min [23] and 16.66 nm/min [24]. The decrease in deposition rate with oxygen flow rate is typical for reactive sputtering and is related to target poisoning [25]. As discussed by Westwood [26], target poisoning occurs when the oxygen flow rate is increased to a certain value where the target surface oxidizes. The formation of the oxide layer has two major effects, (1) limits the arrival rate of Zn atoms and (2) decreases the acceleration of Ar^+ ions towards the target, hence, decreasing the sputtering yield. The sputtering time was increased for the samples prepared at lower deposition rates to keep the thickness of the film close to 500 nm.

Performing sputtering deposition under conditions where the amount of available oxygen is limited, e.g., using a metallic target and low partial pressures of oxygen in the sputtering gas, is known to result in the formation of more "metallic" films, i.e., with a deficiency of oxygen in their stoichiometry, resulting in V_O and zinc interstitials (Zn_i) [27]. Meanwhile, deposition at higher partial pressures of oxygen will improve the film stoichiometry, reducing the number of defects.

The surface chemical composition of the ZnO thin films was studied using XPS to track the formation of point defects. Figure 2 shows the high-resolution spectra of the O 1s region. As seen, the O 1s peak is asymmetric for all the films. This asymmetry indicates the presence of different oxygen species on the surface of the films. The peaks were fitted using the Multi-Peak Fitting package from Igor Pro (WaveMetrics, Lake Oswego, OR, USA), with Gaussian shape peaks and a cubic polynomial function as baseline. No constraints to the fit parameters were applied and the fit interval was between 520 and 539 eV. The peak at low binding energies, 529 eV (O_0), is attributed to oxygen ions (O^{2-}) that are surrounded by zinc atoms with a full supplement of nearest neighbors in the wurtzite structure [28]. The O 1s peak at approximately 531 eV (O_1) is ascribed to O^{2-} ions in the vicinity of V_O [11,29,30], and its relative area can provide a measure of the V_O concentration. The peak at 532 eV (O_2) is related to oxygen species adsorbed on the surface of the films [31].

It is known that the areas under the O 1s peaks provide additional information about the surface composition [13,32]. Figure 3 shows the area of O_0 and O_1 relative to the total area O_{Tot} ($O_{Tot} = O_0 + O_1$) of the oxygen signals, i.e., O_0/O_{Tot} and O_1/O_{Tot}, as a function of the O_2/Ar ratio. The plot shows an increase in the relative areas O_0/O_{Tot} for all O_2/Ar sputtering gas ratios. The increase in the fully supplemented oxygen, O_0, was expected, as the availability of oxygen in the gas resulted in its incorporation in the growing film when the oxygen partial pressure of the sputtering gas was increased. Meanwhile, the relative area O_1/O_{Tot} decreases, which results from a reduction in V_O, as there is more oxygen available for film growth. At 70 % O_2/Ar, the O_0/O_{Tot} ratio shows the largest increase due to the largest reduction in O_1/O_{Tot}, which is the signal related to V_O. Thus, all films contain V_O with a related signal that decreases as the amount of ambient oxygen increases.

Figure 4 a-d shows the SEM micrograph of the ZnO thin films grown at different O_2/Ar ratios. The films have a grain morphology with different shapes and sizes. The averaged grain size, as estimated using ImageJ software tools, was 117.81 nm, 118.15 nm, 127.18 nm and 146.37 nm for the films grow at 20 %, 30 %, 50 % and 70 % respectively. The increase in grain size with increasing O_2/Ar ratio can be attributed to the amount of oxygen available to react with the zinc atoms.

The X-ray diffractograms of the ZnO films are shown in Figure 5. All the films exhibit only one diffraction peak for the (0002) plane, characteristic of a wurtzite structure. This result indicate that oriented ZnO films can be grown in the wurtzite phase and without secondary phases by reactive sputtering with an O_2/Ar ratio as low as 20 % within the instrumental resolution. The (0002) preferred orientation of the ZnO thin films grown on the SiO_2 substrate is due to the self-texturing phenomenon [33].

The (0002) diffraction angle deviates from the ZnO bulk value of 34.44° [33]. This shift towards higher angles indicates a reduction in the interplanar distance d as well as a reduction in the lattice parameter c as the O_2/Ar ratio increases. Figure 6 shows the variation in the lattice parameter c with the O_2/Ar ratio. For the films grown under 20 %, 30 % and 50 % ratios, the lattice parameter c shows values above bulk (5.206 Å), while c is slightly smaller for the film grown under a ratio of 70 %.

The smaller lattice parameter c in the films grown at 70 % O_2/Ar can be explained by an increase in ion bombardment of the growing film as the amount of oxygen increases. Ion bombardment by energetic oxygen species provides forward momentum to the atoms in the growing film [34]. This process produces densification and, if tuned correctly, will shift the lattice parameter by diffusing atoms from a non-equilibrium position to an equilibrium one. Meanwhile, excessive ion bombardment will produce the contrary effect, causing damage and even erosion from the substrate. For the deposition conditions used in our experiments, the plasma gas pressure and target-to-substrate distance, were sufficiently high to prevent excessive damage while shifting the c lattice parameter toward the equilibrium value. Figure 6 also shows the crystallite size, as calculated with Scherrer's equation. The crystallite size increases from 7.383 nm for 20 % to approximately 12.041 nm for samples deposited at larger O_2/Ar ratios.

The smaller crystallite size produced at 20 % O_2/Ar confirms that the amount of oxygen available to the growing film was limited, resulting in a growth process that was controlled by the kinetics of the concentration deficiency of the oxygen reactant. At higher ratios, crystallite growth was controlled by the limited mobility characteristic of the sputtering process at room temperature.

Additional information about the phase structure of the film can be obtained from Raman scattering due to its sensitivity to changes in the microstructure of the material, facilitating the analysis of the crystal quality. Figure 7a shows the Raman spectra with the E_2(low) and E_2(high) phonon modes, which are characteristic of the wurtzite structure. The low-frequency E_2 mode is associated with the vibrations of the zinc sublattice, while the high-frequency E_2 mode is associated with the oxygen sublattice [25]. The intensity of the Raman peaks can be affected by the presence of structural defects, disorder in the films and/or misorientation of the (0002) planes [24]. Thus, a broad and weak E_2(low) peak is due disorder and structural defects that makes the films discontinuous and to point defects present in the films. In addition, the Raman spectra show a band in the range 2800-3000 cm^{-1} in all the films (Figure 7b). This band has previously been assigned to the presence of hydroxyl groups (OH) [36].

Defects with unpaired electrons were studied by EPR at room temperature. Figure 8 shows the EPR spectra for the ZnO thin films grown at various O2/Ar ratios. All the samples show a low-field EPR signal at a resonance field of approximately 336.4 mT, corresponding to a g-factor of 2.00, while the film grown at 20 % O2/Ar shows an additional signal at approximately 343.2 mT with a g-factor of 1.96, indicating that there are two types of paramagnetic centers.

A recent study of paramagnetic centers in thin dioxide nanocrystals [37] has shown that exposing the nanocrystals to water vapor increases the intensity of the EPR signal with g-factor of 2.00, and assigned the signal to OH radicals on their surface. It was proposed that the OH groups arise from the dissociation of water molecules on VO sites at the surface of the films [38].

Based on our results from Raman spectroscopy and the cited reports, the EPR signal with gfactor of 2.00 is attributed to OH groups on the surface of the films.

The signal with a g-factor around 1.96 has been assigned in the literature to VZn [13], Zni [39] and VO [11]. This signal is only observed in the film grown at 20 % O2/Ar and is very weak. At 20 % O2/Ar ratio, a low concentration of VZn is expected due to its high formation energy relative to Vo in an oxygen-deficient environment [40,41], thus, it is unlikely that the signal at 1.96 arises from this defect. For Zni in ZnO, its presence is revealed by high-resolution XPS spectra in the Zn 2p region where it exhibits shoulder-like features at 1024.9 and 1047.11 [42]. In this work, the high-resolution spectrum of the Zn 2p (not shown) reveals that the peaks are symmetric. Also, interstitial zinc is a high mobility species that is favorable to move to a lattice position and it is found to occur exclusively in the 2+ charge state in n-type ZnO [40]. Therefore, the possibility that Zni is the origin of the EPR signal at 1.96 is discarded.

Given that the 20 % O2/Ar film has the largest amount of oxygen vacancies, the observed signal may correspond to a singly ionized charged state of the oxygen vacancy. Oxygen vacancies can exist in three charge states; the neutral VO, the singly ionized VO+ and the doubly ionized state VO2+, where the singly ionized VO+ is the state that produces a paramagnetic signal in EPR [40]. If the EPR signal is associated with VO+, then the fact that is weak and completely disappears for samples with higher O2/Ar ratios can be explained by its low thermal stability.

From first principle calculations performed by Janotti et. al. [40], it was shown that the VO and VO2+ charge states are thermodynamically more stable than VO+. The energy of the singly charged oxygen vacancy is always higher than either VO or VO2+. This explains why we observe a very weak EPR signal, and only in the sample with the largest amount of oxygen vacancies and smallest crystallite size. In the samples with higher O2/Ar ratios, the crystallite size increases, the number of oxygen vacancies decreases, therefore, there is a lower probability of forming VO+. For these samples, the 1.96 EPR signal either disappears or falls below the detection limits of the instrument.

The interaction between the ZnO crystal lattice and the paramagnetic vacancies is another factor that affects the strength of the EPR signal. For example, recent work on the thermal stability of the spin centers in SnO2 [8] has shown that for a constant concentration of spin centers, as the temperature increases the amplitude of the signal decreases while its width increases. The signal width is inversely proportional to the lifetime of the spin-excited state, according to the uncertainty principle. Thus, the lifetime of the spin excited states is highly susceptible to the temperature-induced phonon vibrations. Since the measurements in this work were recorded at room temperature, the shortening of the spin excited state lifetime due to the spin-lattice relaxation will reduce the EPR signal amplitude. Thus, our results are consistent with the VO+ located at the crystallite lattice rather than the surface of the films.

4. Conclusions

In order to investigate the effect of the O_2/Ar ratio in the sputtering gas on the composition, crystallinity, and the formation of surface active sites on ZnO thin films grown by reactive magnetron sputtering, the O_2/Ar ratio was changed from 20 % to 70 %. In terms of structure, the films exhibit a wurtzite phase, as shown by XRD and Raman spectra, with increasing crystallite size as the oxygen partial pressure increases. XPS results show that the film grown at 20 % O_2/Ar ratio has the largest number of oxygen vacancies, Vo, and that the number of vacancies decreases as the O_2/Ar ratio increases.

Vibrational modes associated to hydroxide, OH, bonds are observed in the Raman spectra of all samples. The presence of strong EPR signal, with a g-factor of 2.00, in all the samples is consistent with the formation of hydroxyl groups on the surface of the films, which act as paramagnetic centers. A weak EPR signal, with a g-factor of 1.96, only appears in the film grown at 20 % O2/Ar ratio and, after eliminating other possible sources, assigned to VO+. This assignment is justified because the signal only appears in the sample with the largest amount of oxygen vacancies, VO, and thus, the highest probability of containing singly ionized point defects. These results are consistent with the VO+ located at the crystallite lattice rather than the surface of the films. For the films deposited with higher O2/Ar ratios, the 1.96 EPR signal either disappears or falls below the detection limits of the instrument.

Since the paramagnetic centers are reactive as result of their unpaired electrons, they are of great interest as active sites for gas sensing applications. Therefore, it is expected that the transduction properties of ZnO films grown under different oxygen deficient conditions, and consequently different number of paramagnetic centers acting as active sites, can be tuned for their use as gas sensors.

Acknowledgements

The authors would like to thank Dr. M.B. Jungfleisch and Dr. A. Hoffman of the Magnetic Films group, Argonne National Laboratory for help with EPR measurements, Dr. S. Kumari and Dr. R. Katiyar of the Institute for Functional Nanomaterials, University of Puerto

Rico, for the magnetic measurements and the Molecular Science Research Building for the XRD, Raman and XPS measurements. W.O. like to acknowledge the help of the Instituto de Investigaciones Interdisciplinarias in the University of Puerto Rico at Cayey for their support to his research activities related to this work. This work was supported by the NSF [grant number EPS-01002410]; NSF-CREST [grant numbers 1736093]; and NASA [grant number NNX15AI11H].

Declarations of interest:

None.

REFERENCES

[1] B. Xue, Y. Zou, Uniform distribution of ZnO nanoparticles on the surface of grpahene and its enhanced photocatalytic performance, Appl. Surf. Sci. 440 (2018) 1123–1129. doi:10.1016/j.apsusc.2018.01.299.

[2] M.W. Ahn, K.S. Park, J.H. Heo, J.G. Park, D.W. Kim, K.J. Choi, J.H. Lee, S.H. Hong, Gas sensing properties of defect-controlled ZnO-nanowire gas sensor, Appl. Phys. Lett. 93 (2008) 8–11. doi:10.1063/1.3046726.

[3] J. Wang, R. Chen, L. Xiang, S. Komarneni, Synthesis, properties and applications of ZnO nanomaterials with oxygen vacancies: A review, Ceram. Int. 44 (2018) 7357–7377. doi:10.1016/j.ceramint.2018.02.013.

[4] P.K. Kannan, R. Saraswathi, J.B.B. Rayappan, A highly sensitive humidity sensor based on DC reactive magnetron sputtered zinc oxide thin film, Sensors Actuators A Phys. 164 (2010) 8–14. doi:10.1016/j.sna.2010.09.006.

[5] A. V. Marikutsa, N.A. Vorob´eva, M.N. Rumyantseva, A.M. Gas´kov, Active sites on the surface of nanocrystalline semiconductor oxides ZnO and SnO2 and gas sensitivity, Russ. Chem. Bull. 66 (2017) 1728–1764. doi:10.1007/s11172-017-1949-7.

[6] K. Tabata, T. Kawabe, Y. Yamaguchi, Y. Nagasawa, Chemisorbed oxygen species over the (110) face of SnO2, Catal. Surv. from Asia. 7 (2003) 251–259.

[7] N. Vorobyeva, M. Rumyantseva, E. Konstantinova, D. Grishina, A. Gaskov, Inversion of NH 3 sensor signal and paramagnetic centers of nanocrystalline ZnO(Ga), Procedia Eng. 25 (2011) 296–299. doi:10.1016/j.proeng.2011.12.073.

[8] A. V. Marikutsa, M.N. Rumyantseva, E.A. Konstantinova, T.B. Shatalova, A.M. Gaskov, Active sites on nanocrystalline tin dioxide surface: Effect of palladium and ruthenium oxides clusters, J. Phys. Chem. C. 118 (2014) 21541–21549. doi:10.1021/jp5071902.

[9] A.K. Das, A. Srinivasan, Evidence of oxygen defect induced ferromagnetism in heat treated electrospun ZnO nanowires, J. Magn. Magn. Mater. 404 (2016) 190–196. doi:10.1016/j.jmmm.2015.12.032.

[10] D.E. Motaung, P.R. Makgwane, S.S. Ray, Induced ferromagnetic and gas sensing properties in ZnO-nanostructures by altering defect concentration of oxygen and zinc vacancies, Mater. Lett. 139 (2015) 475–479. doi:10.1016/j.matlet.2014.10.073.

[11] X. Xu, C. Xu, J. Dai, J. Hu, F. Li, S. Zhang, Size dependence of defect-induced room temperature ferromagnetism in undoped ZnO nanoparticles, J. Phys. Chem. C. 116 (2012) 8813–8818. doi:10.1021/jp3014749.

[12] P. Jakes, E. Erdem, Finite size effects in ZnO nanoparticles: An electron paramagnetic resonance (EPR) analysis, Phys. Status Solidi. 5 (2011) 56–58. doi:10.1002/pssr.201004450.

[13] G.H. Mhlongo, D.E. Motaung, S.S. Nkosi, H.C. Swart, G.F. Malgas, K.T. Hillie, B.W. Mwakikunga, Temperature-dependence on the structural, optical, and paramagnetic properties of ZnO nanostructures, Appl. Surf. Sci. 293 (2014) 62–70. doi:10.1016/j.apsusc.2013.12.076.

[14] L. Zhang, L. Yin, C. Wang, N. Lun, Y. Qi, D. Xiang, Origin of visible photoluminescence of ZnO quantum dots: Defect-dependent and size-dependent, J. Phys. Chem. C. 114 (2010) 9651–9658. doi:10.1021/jp101324a.

[15] A.B. Djurišić, W.C.H. Choy, V.A.L. Roy, Y.H. Leung, C.Y. Kwong, K.W. Cheah, T.K.G. Rao, W.K. Chan, H.F. Lui, C. Surya, Photoluminescence and electron paramagnetic resonance of ZnO tetrapod structures, Adv. Funct. Mater. 14 (2004) 856–864. doi:10.1002/adfm.200305082.

[16] A. Hausmann, B. Schallenberger, Interstitial oxygen in zinc oxide single crystals, Zeitschrift Für Phys. B Condens. Matter Quanta. 31 (1978) 269–273. doi:10.1007/BF01352351.

[17] S. Ning, P. Zhan, W.-P. Wang, Z.-C. Li, Z.-J. Zhang, Defect characterization and magnetic properties in un-doped ZnO thin film annealed in a strong magnetic field, Chinese Phys. B. 23 (2014) 127503. doi:10.1088/1674-1056/23/12/127503.

[18] S. Youssef, P. Combette, J. Podlecki, R. Al Asmar, A. Foucaran, Structural and Optical Characterization of ZnO Thin Films Deposited by Reactive rf Magnetron Sputtering, Cryst. Growth Des. 9 (2008) 1088–1094. doi:10.1021/cg800905e.

[19] U.C. Singh, P.K. Basu, C.N.R. Rao, Oxygen Effecton Structural and Optical Properties of ZnO Thin Films Deposited by RF Magnetron Sputtering, J. Mol. Struct. THEOCHEM. 87 (1982) 125–132. doi:10.1016/0166-1280(82)80046-8.

[20] E. Muchuweni, T.S. Sathiaraj, H. Nyakotyo, Effect of O2/Ar flow ratio on Ga and Al codoped ZnO thin films by rf sputtering for optoelectronic device fabrication, Mater. Res. Bull. 95 (2017) 123–128. doi:10.1016/j.materresbull.2017.07.029.

[21] V.V. Sasi, A. Iqbal, K. Chaik, P. Tanner, A. Iacopi, F. Mohd-Yasin, RF Sputtering of ZnO (002) Thin Films on Top of 3C-SiC-on-Si (100) Substrates for Low Cost Piezoelectric Devices, Procedia Eng. 168 (2016) 1086–1089. doi:10.1016/j.proeng.2016.11.346.

[22] M.H. Mamat, M.F. Malek, N.N. Hafizah, M.N. Asiah, A.B. Suriani, A. Mohamed, N. Nafarizal, M.K. Ahmad, M. Rusop, Effect of oxygen flow rate on the ultraviolet sensing properties of zinc oxide nanocolumn arrays grown by radio frequency magnetron sputtering, Ceram. Int. 42 (2016) 4107–4119. doi:10.1016/j.ceramint.2015.11.083.

[23] Z.B. Fang, Z.J. Yan, Y.S. Tan, X.Q. Liu, Y.Y. Wang, Influence of post-annealing treatment on the structure properties of ZnO films, Appl. Surf. Sci. 241 (2005) 303–308. doi:10.1016/j.apsusc.2004.07.056.

[24] S. Singh, R.S. Srinivasa, S.S. Major, Effect of substrate temperature on the structure and optical properties of ZnO thin films deposited by reactive rf magnetron sputtering, Thin Solid Films. 515 (2007) 8718–8722. doi:10.1016/j.tsf.2007.03.168.

[25] B. Amrani, S. Hamzaoui, Characterization of ZnO films prepared by reactive sputtering at different oxygen pressures, Catal. Today. 89 (2004) 331–335. doi:10.1016/j.cattod.2003.12.014.

[26] W.D. Westwood, Basics of Reactive Sputtering, in: Sputter Depos., AVS, New York, 2003: pp. 213–217.

[27] R. Hong, H. Qi, J. Huang, H. He, Z. Fan, J. Shao, Influence of oxygen partial pressure on the structure and photoluminescence of direct current reactive magnetron sputtering ZnO thin films, Thin Solid Films. 473 (2005) 58–62. doi:10.1016/j.tsf.2004.06.159.

[28] Z.-B. Gu, M.-H. Lu, J. Wang, D. Wu, S.-T. Zhang, X.-K. Meng, Y.-Y. Zhu, S.-N. Zhu, Y.-F. Chen, X.-Q. Pan, Structure, optical, and magnetic properties of sputtered manganese and nitrogen-codoped ZnO films, Appl. Phys. Lett. 88 (2006) 082111. doi:10.1063/1.2178466.

[29] J.C.C. Fan, J.B. Goodenough, X-ray photoemission spectroscopy studies of Sn-doped indium-oxide films, J. Appl. Phys. 48 (1977) 3524–3531. doi:10.1063/1.324149.

[30] E. Fazio, S. Patanè, S. Scibilia, A.M. Mezzasalma, G. Mondio, F. Neri, S. Trusso, Structural and optical properties of pulsed laser deposited ZnO thin films, Curr. Appl. Phys. 13 (2013) 710–716. doi:10.1016/j.cap.2012.11.010.

[31] L. Jing, Z. Xu, J. Shang, X. Sun, W. Cai, H. Guo, The preparation and characterization of ZnO ultrafine particles, Mater. Sci. Eng. A. 332 (2002) 356–361. doi:10.1016/S09215093(01)01801-9.

[32] M.M. Can, S. Ismat Shah, M.F. Doty, C.R. Haughn, T. Fırat, Electrical and optical properties of point defects in ZnO thin films, J. Phys. D. Appl. Phys. 45 (2012) 195104. doi:10.1088/0022-3727/45/19/195104.

[33] D.-S. Kim, J.-H. Park, S.-J. Lee, K.-J. Ahn, M.-S. Lee, M.-H. Ham, W. Lee, J.-M. Myoung, Effects of oxygen concentration on the properties of Al-doped ZnO transparent conductive films deposited by pulsed DC magnetron sputtering, Mater. Sci. Semicond. Process. 16 (2013) 997–1001. doi:10.1016/j.mssp.2013.02.012.

[34] G. Abadias, E. Chason, J. Keckes, M. Sebastiani, G.B. Thompson, E. Barthel, G.L. Doll, C.E. Murray, C.H. Stoessel, L. Martinu, Review Article: Stress in thin films and coatings: Current status, challenges, and prospects, J. Vac. Sci. Technol. A Vacuum, Surfaces, Film. 36 (2018) 020801. doi:10.1116/1.5011790.

[35] Ü. Özgür, Y.I. Alivov, C. Liu, A. Teke, M.A. Reshchikov, S. Doğan, V. Avrutin, S.J. Cho, H. Morkọ, U. Ozgur, Y.I. Alivov, C. Liu, A. Teke, M.A. Reshchikov, S. Dogan, V. Avrutin, S.J. Cho, H. Morkoç, A comprehensive review of ZnO materials and devices, J. Appl. Phys. 98 (2005) 1–103. doi:10.1063/1.1992666.

[36] S. Paul, P.G. Harris, C. Pal, A.K. Sharma, A.K. Ray, Low cost zinc oxide for memristors with high On-Off ratios, Mater. Lett. 130 (2014) 40–42. doi:10.1016/j.matlet.2014.05.071.

[37] E.A. Konstantinova, I.S. Pentegov, A. V. Marikutsa, M.N. Rumyantseva, A.M. Gaskov, P.K. Kashkarov, EPR study of nanocrystalline tin dioxide, Phys. Status Solidi Curr. Top. Solid State Phys. 8 (2011) 1957–1960. doi:10.1002/pssc.201000140.

[38] H. Noei, H. Qiu, Y. Wang, E. Löffler, C. Wöll, M. Muhler, The identification of hydroxyl groups on ZnO nanoparticles by infrared spectroscopy, Phys. Chem. Chem. Phys. 10 (2008) 7092–7097. doi:10.1039/b811029h.

[39] H. Zeng, G. Duan, Y. Li, S. Yang, X. Xu, W. Cai, Blue luminescence of ZnO nanoparticles based on non-equilibrium processes: Defect origins and emission controls, Adv. Funct. Mater. 20 (2010) 561–572. doi:10.1002/adfm.200901884.

[40] A. Janotti, C.G. Van De Walle, Native point defects in ZnO, Phys. Rev. B - Condens. Matter Mater. Phys. 76 (2007) 1–22. doi:10.1103/PhysRevB.76.165202.

[41] A. Janotti, C.G. Van de Walle, Fundamentals of zinc oxide as a semiconductor, Reports Prog. Phys. 72 (2009) 126501. doi:10.1088/0034-4885/72/12/126501.

[42] F. Kayaci, S. Vempati, I. Donmez, N. Biyikli, T. Uyar, Role of zinc interstitials and oxygen vacancies of ZnO in photocatalysis: A bottom-up approach to control defect density, Nanoscale. 6 (2014) 10224–10234. doi:10.1039/c4nr01887g.

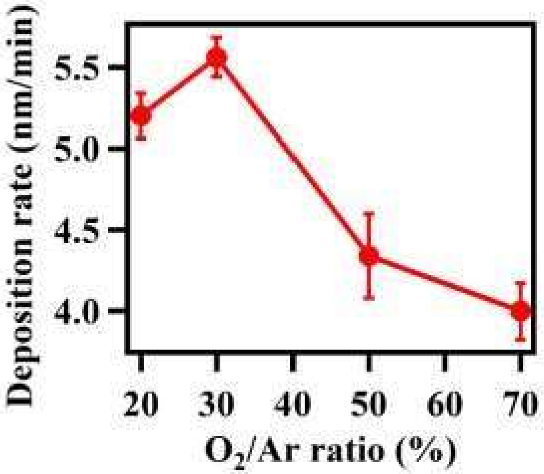

Fig. 1. Deposition rate of ZnO thin films as a function of the oxygen to argon ratio.

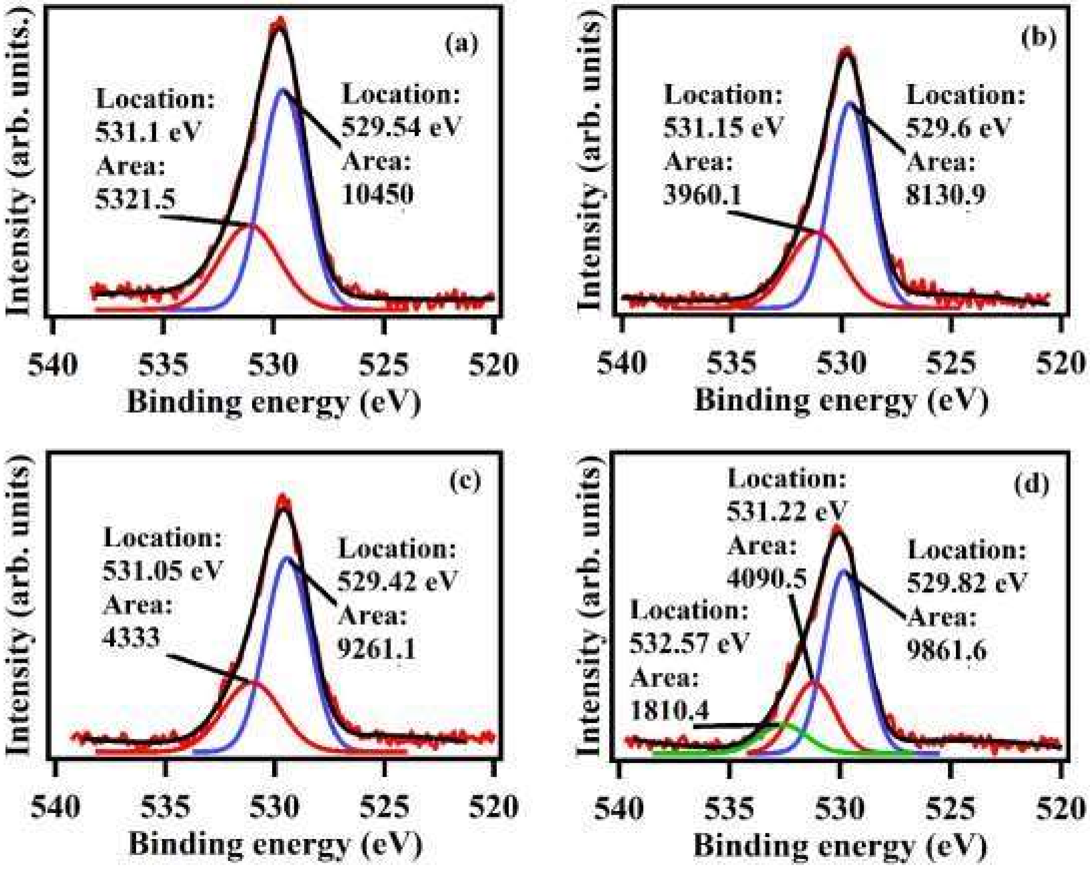

Fig. 2. High-resolution scan of the O 1s peak for ZnO thin films grown under O_2/Ar ratios of (a) 20 %, (b) 30 %, (c) 50 % and (d) 70 %.

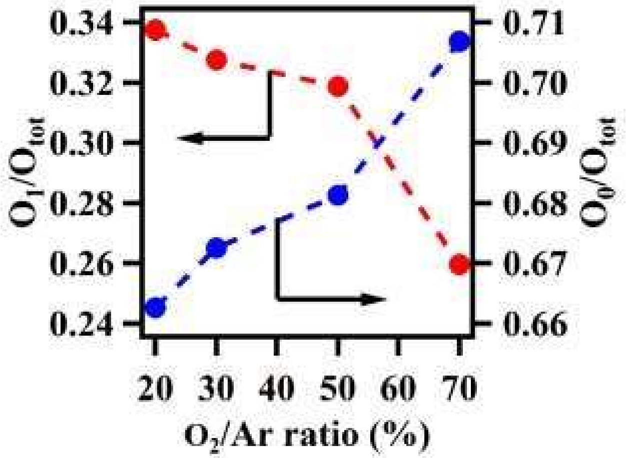

Fig. 3. Comparison between the O_0/O_{Tot} area ratio and O_1/O_{Tot} ratios. The dashed lines are provided as visual aids.

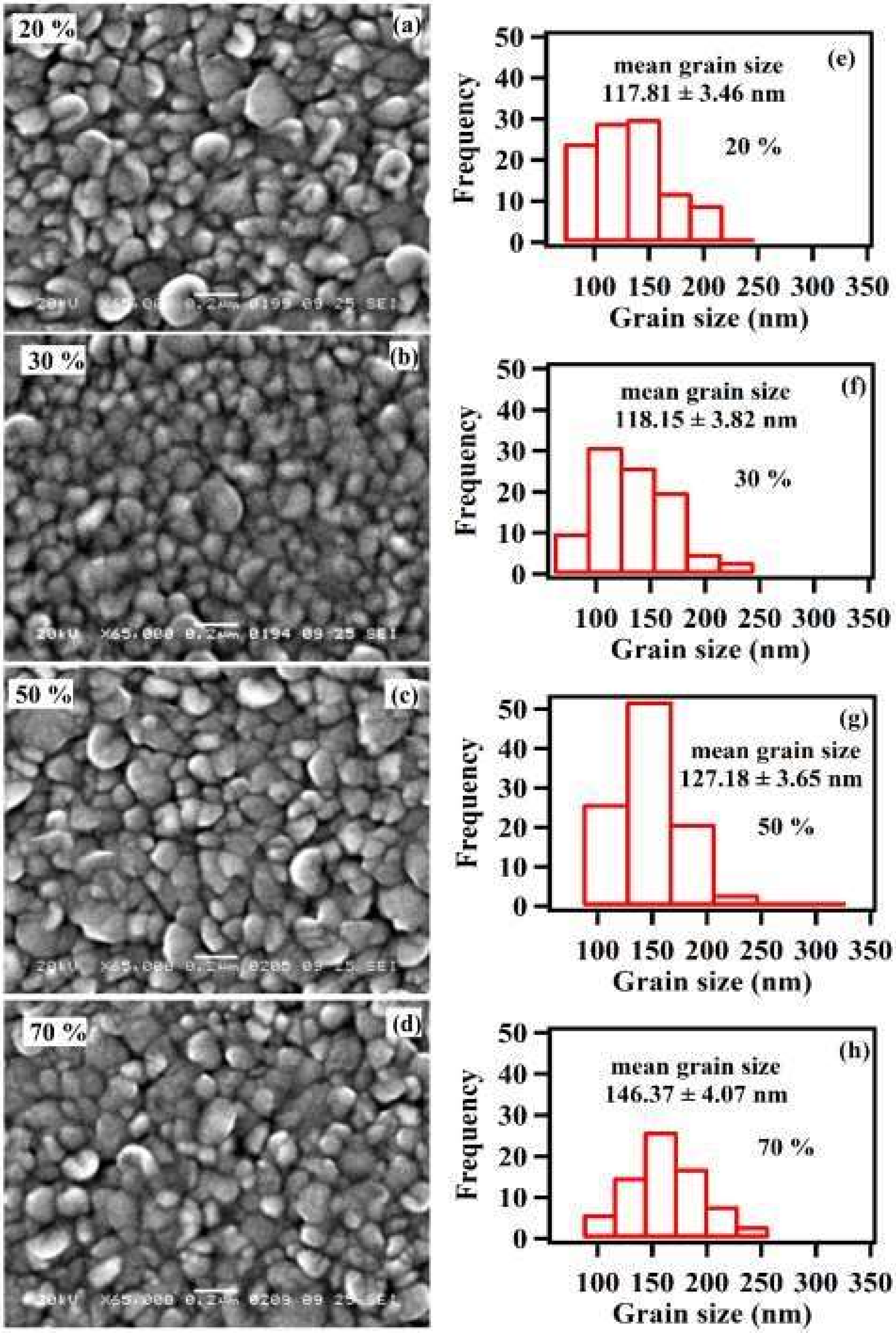

Fig. 4. (a-d) SEM micrographs for ZnO/SiOx thin films grown under 20 %, 30 %, 50 % and 70 % O_2/Ar ratios at T_{sub} = 25 °C, (e-f) grain size distribution.

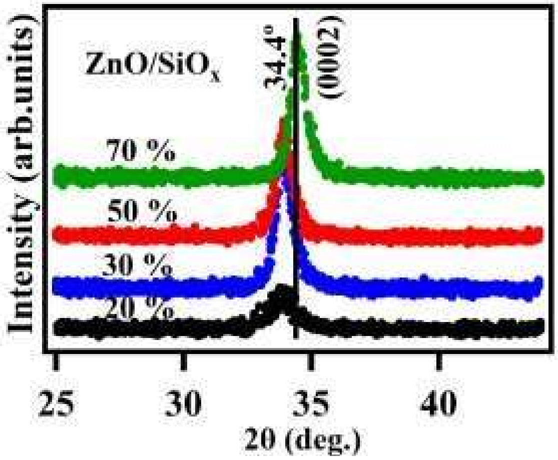

Fig. 5. X-ray diffraction patterns for ZnO/SiO$_x$ thin films grown under 20 %, 30 %, 50 % and 70 % O_2/Ar ratios at T_{sub} = 25 °C.

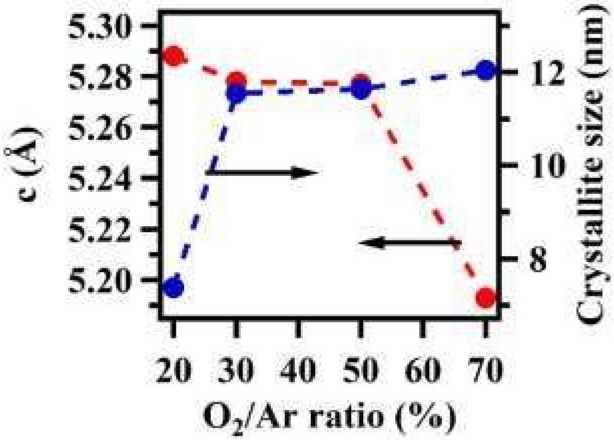

Fig. 6. Lattice parameter c and crystallite size as a function of the O_2/Ar ratio.

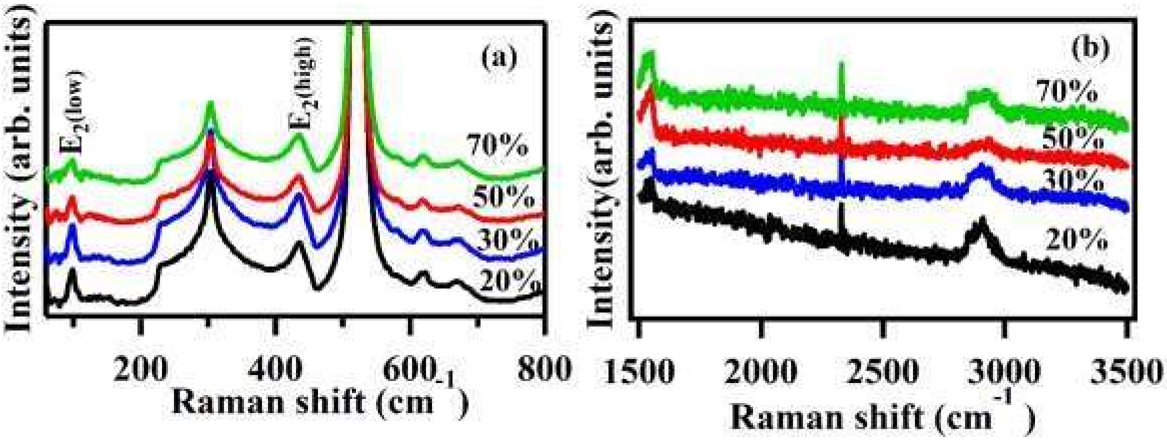

Fig. 7. (a) Raman spectra of ZnO thin films grown under O_2/Ar ratios of 20 %, 30 %, 50 % and 70 %.

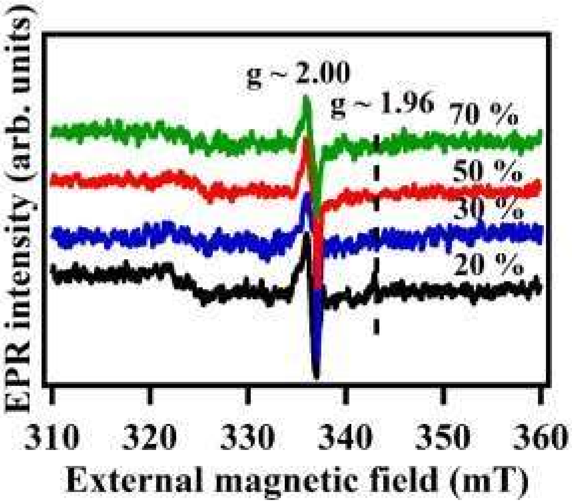

Fig. 8. Room-temperature EPR spectra for ZnO thin films grown at O_2/Ar ratios of 20 %, 30 %, 50 % and 70 % in the sputtering gas.

Table 1.

Deposition parameters for undoped ZnO thin films grown by reactive magnetron sputtering.

O_2/Ar ratio (%)	Oxygen flow (SCCM)	Argon flow (SCCM)	Power (W)	Dep. Pressure (Pa)	T_{sub} ºC	Deposition rate (nm/min)
20	8	32	40	1.33	25	5.20 ± 0.14
30	12	28	40	1.33	25	5.56 ± 0.12
50	20	20	40	1.33	25	4.34 ± 0.26
70	20	8.5	40	1.33	25	4.00 ± 0.17